DETECTION OF SHORT-PERIOD CORONAL OSCILLATIONS DURING THE TOTAL SOLAR ECLIPSE OF 24 OCTOBER, 1995

JAGDEV SINGH, R. COWSIK, A. V. RAVEENDRAN, S. P. BAGARE, A. K. SAXENA, K. SUNDARARAMAN, VINOD KRISHAN, NAGARAJA NAIDU, J. P. A. SAMSON and F. GABRIEL
Indian Institute of Astrophysics, Bangalore 560034, India

(Received 7 February, 1996; in final form 29 August, 1996)

Abstract. An experiment to search for short-period oscillations in the solar corona was conducted during the total solar eclipse of 1995 October 24 at Kalpi, India. The intensity in the continuum, centred around 5500 Å and with a passband having a half-width of 240 Å, was recorded at a counting rate of 20 Hz using a thermoelectric-liquid cooled photomultiplier. The power-spectrum analysis of the data reveals that most of the power is contained in 6 frequencies below 0.2 Hz. A least-square analysis gives the periods of the 6 frequency components to be 56.5, 19.5, 13.5, 8.0, 6.1, and 5.3 s. These oscillations are found to be sinusoidal, and their amplitudes are found to lie in the range 0.2–1.3% of the coronal brightness. Assuming these oscillations to be fast magnetosonic modes, the calculations indicate the availability of enough flux for the heating of the active regions in the solar corona.

1. Introduction

The study of coronal oscillations is important since these oscillations could be responsible for the heating of the solar corona. They can be observed either as the intensity oscillations of a spectral line or of the continuum, or as the velocity oscillations in the Doppler profiles. The velocity oscillations without the accompaniment of intensity oscillations are interpreted as non-compressional Alfvén waves, whereas the intensity oscillations accompanied by velocity oscillations are interpreted as compressional magnetoacoustic waves.

There is a large body of literature on the theoretical studies of these oscillations (e.g., Porter, Klimchuk, and Sturrock 1994, and references therein; Zirker, 1995; Cargill, 1995). A number of attempts have been made to detect periodic oscillations or waves in the corona, but the results are not conclusive. They differ widely in all the four parameters: the integrated emission line intensity, the line-width, the line-of-sight Doppler velocity and the asymmetry of the line profile, as the case may be. Koutchmy, Zugzda, and Locans (1983) reported Doppler velocity oscillations with periods near 300, 80, and 43 s, but found no prominent intensity fluctuations from the measurements of the green coronal line at 5303 Å using a coronagraph. Analysis of the green and red coronal line intensities obtained with a photoelectric photometer and a coronagraph by Rušin and Minarovjech (1991) indicated oscillations with periods around 300, 112, 60, and 40 s. Liebenberg and Hoffman (1974) found a 300 s oscillation from their Concorde observations

Solar Physics **170:** 235–252, 1997.

obtained during the total eclipse of 1973; no shorter period oscillations could be detected because of the sampling rate used.

Soon after the acoustic-wave-heating models for the corona were discarded because of OSO-8 observations, and several theoretical studies (Stein and Leibacher, 1974; Ionson, 1978; Hollweg, 1981) emphasizing the importance of looking at coronal waves in the short period range were reported, Pasachoff made observations during a number of eclipses starting with the Indian eclipse of 1980. Pasachoff and Landman (1984) and Pasachoff and Ladd (1987) detected excess power in the 0.5 -2 Hz range at the level of 1% in the coronal green line. Pasachoff's observations were mostly confined to the green coronal line using apertures with 2.5 and 5 arc sec diameters, isolating small regions of the solar corona.

With the background of such observations, we decided to conduct an experiment complementary to that of Pasachoff during the total solar eclipse of 1995 October 24 using a larger aperture to isolate 1.5 arc min region of the corona and with a broader bandpass filter in the coronal continuum radiation. We used only one photometer during this eclipse because of the exploratory nature of the experiment. Our observations indicate the presence of intensity oscillations with several frequency components ranging from about 0.2 Hz to about 0.02 Hz. These could provide a significant impetus to the wave-heating theories in particular and to coronal physics in general.

2. Instrumentation

The Indian Institute of Astrophysics set up camps at two sites, one at Nim Ka Thana (latitude $= 27^\circ 44.6'$ N, longitude $= 75^\circ 48.5'$ E) in Rajasthan and the other at Kalpi ($26^\circ 08.0'$ N, $79^\circ 45.0'$ E) in Uttar Pradesh for the observations. The photometric observations in search of the suspected brightness oscillations in the solar corona were performed at the Kalpi site.

A stepper motor-driven coelostat of 30 cm aperture was used to collect the light from the Sun which in turn was reflected horizontally with the help of a second mirror of 15 cm aperture. The telescope objective was a 10 cm Zeiss achromatic doublet having a focal length of 100 cm. A conventional single channel photometer was mounted horizontally with its diaphragm in the focal plane of the telescope. The 0.5 mm diameter diaphragm used subtended an angle of 1.5 arc min in the sky. With an interference filter of 25 mm diameter placed immediately behind the diaphragm a spectral band of half-width ≈ 240 Å around 5500 Å was isolated for the measurement of coronal intensity.

The photons were detected using a Thorn EMI 9658R photomultiplier tube with the cathode kept at -1600 V. The photometer had a Fabry lens in the light beam in order to reduce the problems associated with the nonuniform sensitivity across the surface of the photocathode. The PMT was mounted in a thermoelectric-liquid heat exchanged Thorn EMI model TE 104RF housing and it was cooled by circulating

water at ambient temperature $\approx 15^{\circ}$ C. The pulse amplifier discriminator was a Thorn EMI Type AD 100 with a dead time of 100 ns. The data acquisition was made with a PC-based, locally developed photon counting system. The digital counter used has a bandwidth of 100 MHz.

3. Observations

The HT supply to the PMT was kept on continuously for more than 15 hours for stabilizing the dark current and the cooling system was turned on about 4 hours before the event. The dark counts before and after the observations were found to be below 250 s^{-1}. A region of the corona at a position angle of 65° at 1.25 $R_{\odot}$ was selected so that an appreciable signal could be obtained during the total phase of the eclipse, and the diaphragm was centred visually around this region. The observations were begun at 03:06:19 UT and ended at 03:08:06 UT. The photon counts were recorded continuously with an integration time of 50 ms. The tracking rate of the stepper motor was adjusted to ensure negligible drift of the image in the E–W direction. The drift in the solar image as a result of the changes in the declination of the sun and errors in the polar axis alignment was less than 1 arc sec per minute. Visually, the sky transparency appeared good and steady throughout the eclipse period. Here, we note that the skies were extremely clear at the site throughout 23–25 October. In order to check the performance of the instrumental setup we made several test runs on the sky brightness during the previous evening twilight.

We have restricted our analysis to the 943 brightness values obtained between 03:06:31 UT and 03:07:19 UT, which we believe are free from any contamination from the photospheric light; these values are plotted in Figure 1. The times used in the plots and the analysis are reckoned from 03:06:31.2 UT.

The highest count rate registered during the total phase of the eclipse is only around 0.37 MHz. The dead-time effects are expected to be negligible at these count rates as the response frequency of the pulse amplifier discriminator was 10 MHz and that of the counter was 100 MHz.

4. Data Analysis and Results

During the total phase of the eclipse the observed counts showed a variability of $\approx$ 1000 counts/50 ms about a mean level of 17 700 counts/50 ms, i.e., at the 6% level. An inspection of Figure 1 clearly reveals the variation in the coronal brightness. In order to detect and isolate the periodic components, the data were Fourier analyzed using the technique of Discrete Fourier Transform (DFT), developed by Deeming (1975).

The DFT of a time series is the convolution of its Fourier Transform with a spectral window defined by the data window over which the sampling is done. The

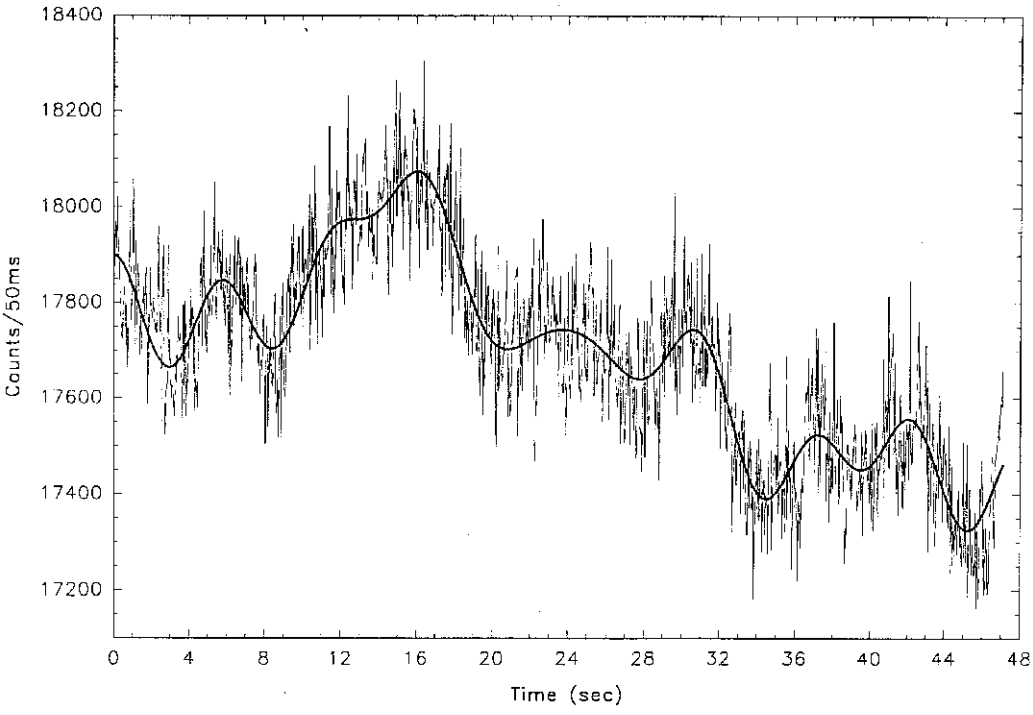

Figure 1. Thin, spiky curve shows the observed data and the smooth, thick curve the computed ones using the 6 frequency components listed in Table I. The time plotted along the x-axis is reckoned from 03:06:31.2 UT.

spectral window is calculated from the times of observation. If the data are sampled at equally spaced intervals, as in the present case, the corresponding power spectral window is simple, and the identification of frequencies with significant power becomes direct.

Before subjecting the data to the technique of DFT, they were not modified in any way other than the subtraction of the arithmetic mean. The resulting amplitude spectrum of the coronal brightness in the frequency interval 0.0−1.0 Hz is shown in Figure 2. The first peak in the figure is due to the large amplitude, low-frequency component evident in the data. We find from the amplitude spectrum that most of the remaining power is contained in 5 frequencies, namely, 0.050, 0.073, 0.125, 0.162, and 0.190 Hz. In order to evaluate the threshold power and hence the statistical significance of the above peaks in the power spectrum we used the technique given in Groth (1975). The histogram of 4710 power values calculated in the range 0−10 Hz is shown in Figure 3 where the logarithm to base 10 of the number of frequency bins is plotted against the corresponding power interval. The straight line represents the exponential distribution of power anticipated from an incoherent background. The known distribution of power and the number of frequency bins considered can be used to establish the threshold power corresponding to any

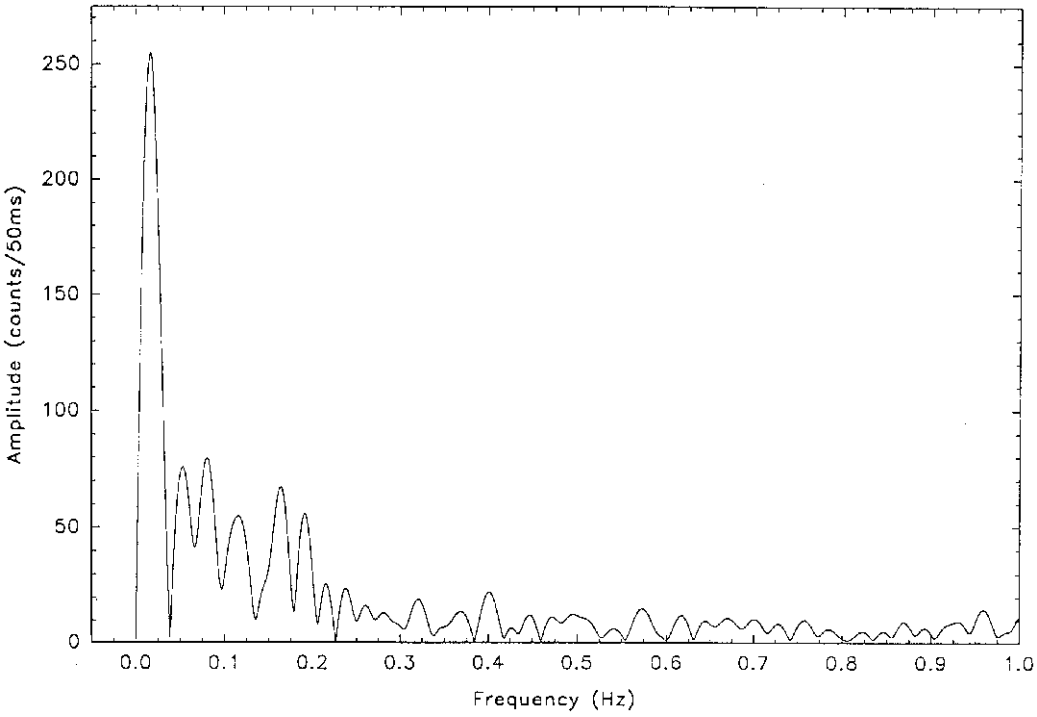

Figure 2. Amplitude spectrum in the frequency interval 0–1 Hz computed from the data. Note that most of the power is contained in the 6 frequency components shortward of 0.2 Hz.

percent confidence level. We find that in the absence of any true signal the probability of a frequency bin to have a power larger than 380 (counts/50 ms)^2 is 0.02%, which means that any amplitude (square root of power) larger than the threshold of 19.5 counts/50 ms is significant above 99.98% confidence level. The amplitudes of the above five frequency components are so large when compared to this threshold that they are significant almost at 100% confidence level.

The presence of peaks in the power spectrum with amplitudes significantly larger than the noise level does not necessarily indicate the presence of coherent brightness modulation with the corresponding periodicities. This is especially true when the data length is short, as in the present case. The peaks appearing in the power spectrum could as well be resulting from stochastic events of various time scales occurring at different time intervals. In what follows we demonstrate the extremely sinusoidal nature and coherence of the above five components during the observational period.

If all the oscillatory components identified are present over the entire data length, a piece-wise analysis of the same would yield similar power spectra. The amplitude spectra in the 0.0–0.4 Hz interval of three slightly overlapping subsets of the data series are plotted in Figures 4(a–c). The low-frequency trend seen in the data was

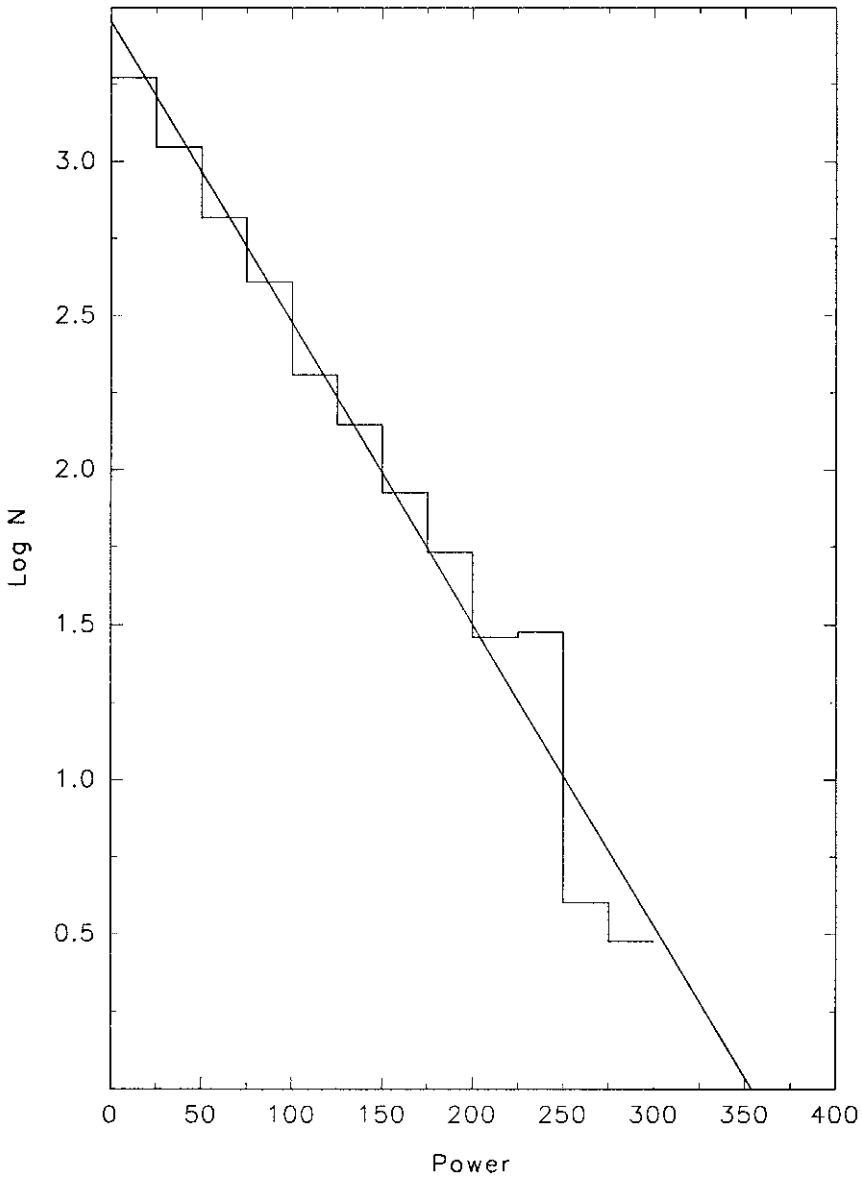

Figure 3. Plot of logarithm to base 10 of the number of frequency bins against the corresponding power interval. The straight line is the exponential distribution expected due to an incoherent background. The unit of power is (counts/50 ms)^2.

removed by subtracting a 56.5 s period sinusoidal modulation. The power spectrum of the entire detrended data series is also shown in the figures for comparison. The shorter lengths of the subsets result in lower resolution power spectra, thereby merging the nearby components. Nevertheless, it is clear from Figures 4(a–c) that

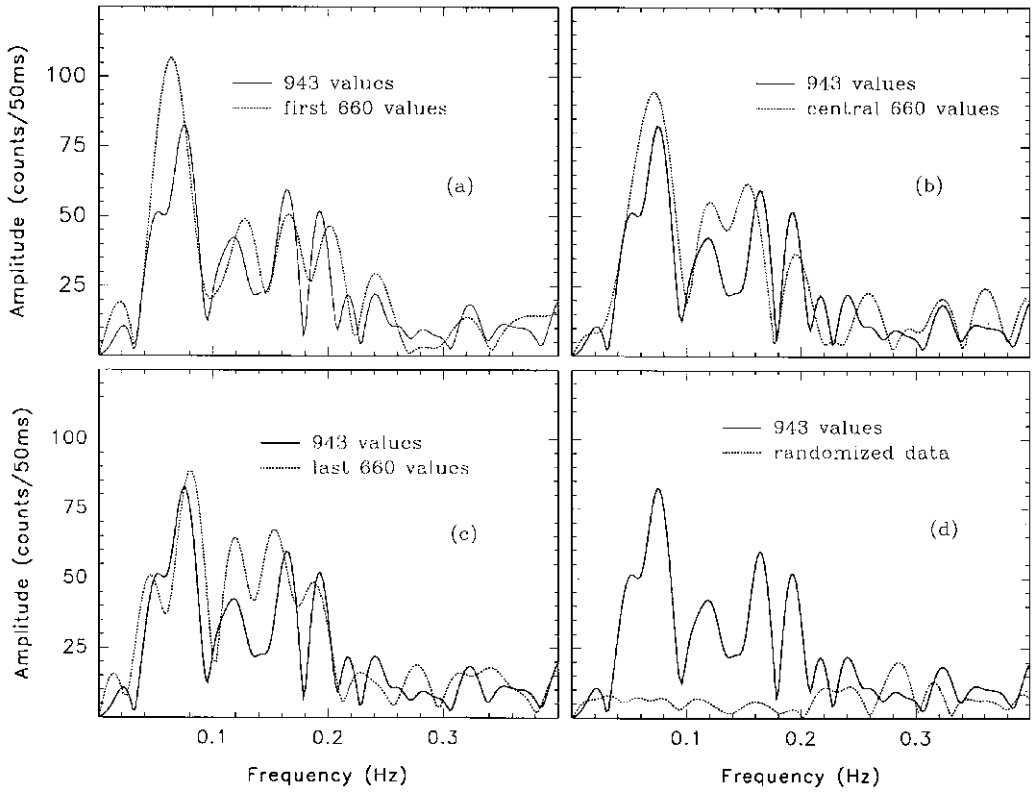

Figure 4. (a–c) Amplitude spectra of three subsets of the original data. (d) Amplitude spectrum of randomized data. For comparison the amplitude spectrum of the whole data set is given in each figure. The low-frequency trend was removed before the Fourier analysis.

the amplitude spectra of the subsets closely agree and the prominent peaks in the spectrum of the individual subseries are the same as the five significant frequency components present in the whole series. We have also calculated the DFT of a new series obtained by randomizing the detrended data. The resulting amplitude spectrum is shown in Figure 4(d); it exhibits no significant peaks in the frequency region where the original series shows large amplitude peaks.

Because of the presence of noise resulting from the incoherent background and the interference from the side lobes of nearby peaks the phases and amplitudes of the components derived from the real and imaginary parts of the spectrum would not be accurate. We used the method of least-squares to derive the frequencies, amplitudes and the times of maximum of the six significant components identified in the power spectrum. These constitute 18 unknowns which were solved simultaneously using the original data, and their values thus obtained are given in Table I along with their probable errors; the mean brightness level was also treated as an unknown in the least-square solution.

Table I
Periodicities identified in the data (mean of input data = 17677 ± 5 counts/50 ms)

No.	Frequency (Hz)	Period (s)	Amplitude (counts/50 ms)	Amplitude % coronal brightness	Time of maximum (s)
1	0.0177 ± 0.0004	56.48 ± 1.44	232 ± 4	1.31 ± 0.02	13.4 ± 1.4
2	0.0512 ± 0.0017	19.52 ± 0.66	48 ± 4	0.27 ± 0.02	15.3 ± 0.6
3	0.0738 ± 0.0009	13.54 ± 0.17	85 ± 4	0.48 ± 0.02	14.8 ± 0.2
4	0.1246 ± 0.0012	8.02 ± 0.08	47 ± 4	0.26 ± 0.02	7.2 ± 0.1
5	0.1629 ± 0.0013	6.14 ± 0.05	54 ± 4	0.30 ± 0.02	5.7 ± 0.1
6	0.1896 ± 0.0020	5.27 ± 0.06	36 ± 4	0.20 ± 0.02	5.5 ± 0.1

The coronal brightness computed using the frequency components listed in Table I is also plotted in Figure 1. The agreement between the computed and the observed brightness variations is excellent over the entire data length. The standard deviation in the observed counts arising from the statistical fluctuations in the photon arrival rate is around 130 counts/50 ms. To bring out the very close agreement in the observed and computed variations, in Figure 5(a) we have re-plotted the computed variations along with the observed data after re-binning them over 0.5 s time interval. The standard deviation in the observed counts from the photon noise is now reduced to 40 counts/50 ms. It is clear that the observed counts are distributed symmetrically about the computed values and the scatter is only of the order expected from the standard deviation.

In Figure 5(b) we have plotted the residuals in the observed brightness after removing the contributions from the components with periods 19.5, 13.5, 8.0, 6.1, and 5.3 s, using the parameters given in Table I. The residuals in this case are expected to show only the 56.5 s modulation component present in the data. Before plotting, the residuals were binned over 0.5 s to reduce the spikiness. The contribution from the 56.5 s period modulation component expected from its parameters given in Table I, is also plotted in the same figure. The agreement between the observed and the computed variations is excellent. Despite the fact that the data length covers only 6/7 of the period involved, we could determine the amplitude, frequency, and input phase fairly accurately because of the extremely sinusoidal nature of the modulation. Similarly, the contributions from the 19.5, 13.5, 8.0, 6.1, and 5.3 s modulation components are plotted in Figures 5(c–g), along with the residuals in the coronal brightness obtained after removing the contributions from all the other components. Again the residuals were averaged over 0.5 s before plotting in the respective figures. Over the entire data length the scatter in the residual coronal brightness about each modulation component computed from its parameters is similar and is comparable to that expected from the photon noise (σ = 40 counts/50 ms). This implies that the 6 components

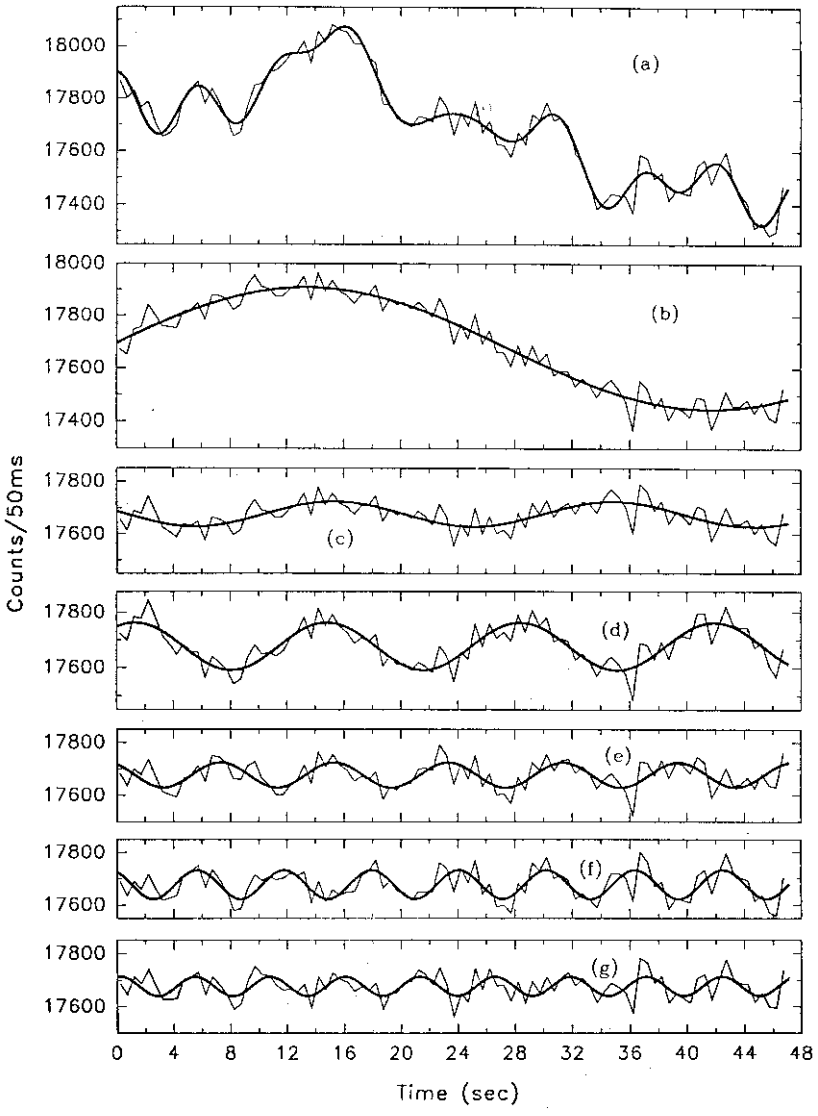

Figure 5. (a) Thin line shows the plot of observations after re-binning over 0.5 s and the thick line the computed curve using the 6 frequency components listed in Table I. (b) Thick line shows the contribution of the 56.5 s component computed using its parameters given in Table I and the thin line the residuals obtained after removing the contributions from all the other components. The residuals are re-binned over 0.5 s before plotting. (c–g) same as (b), but for the 19.5, 13.5, 8.0, 6.1, and 5.3 s components, respectively. The time is reckoned as in Figure 1.

of modulation identified in the coronal brightness are extremely sinusoidal with negligible phase shifts during the interval covered by the observations.

The component with a 5.3 s period, the shortest period identified, has an amplitude of 36 ± 4 counts/50 ms, comparable to the scatter in the residual brightness

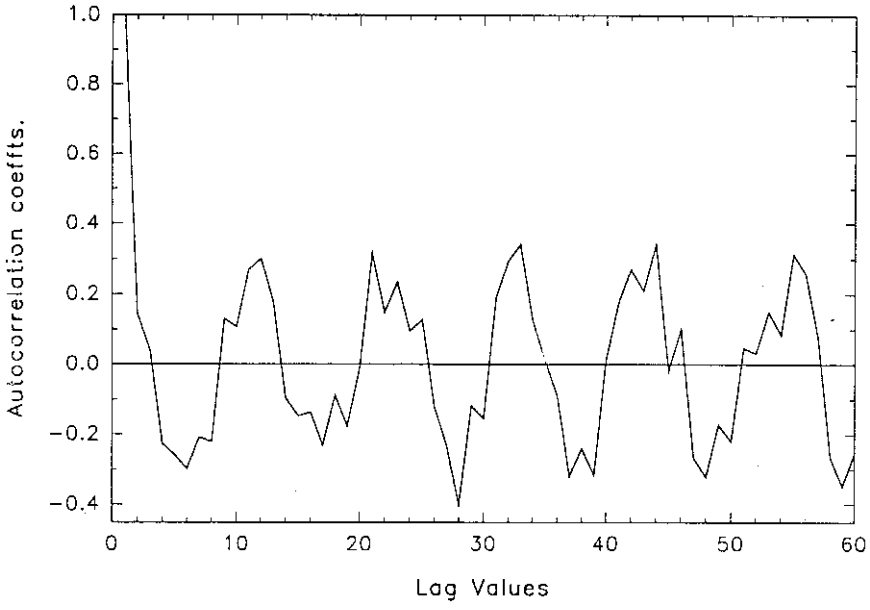

Figure 6. Plot of the autocorrelation coefficients calculated from the residuals obtained after the removal of the contributions from the first 5 frequency components listed in Table I against the corresponding lag values.

arising from the photon noise. However, the modulation by a sinusoidal component present in the residual is apparent in Figure 5(g). To demonstrate further the coherence of the 5.3 s component, we also performed an autocorrelation analysis of these residuals, obtained after removing the contributions from all the components with longer periods. In this case also we averaged the residuals over 0.5 s intervals, resulting in 94 data points. The autocorrelation coefficients are plotted in Figure 6 against the lag values which are in steps of 0.5 s. It is evident from the figure that the autocorrelation coefficient shows a clear periodic pattern with a nearly constant amplitude even beyond 60 lag values, indicating the coherence of the 5.3 s component.

In the following we discuss and rule out the possibility of non-coronal oscillation mechanisms producing the above observed brightness variations.

The sky brightness, which was recorded during the previous evening twilight with the same instrumental setup, is plotted in Figure 7. The observations span over 98 s, twice the span of coronal observations. We calculated the DFT for the entire data set and also for a subset having a data length equal to that of the coronal brightness data. In each case the linear trend arising from the rapid reduction in the sky brightness was removed before the computation of the DFT. The DFT of the entire time series is plotted in Figure 8(a). The power spectrum is noisy but for the presence of two peaks at the short frequency end. The first peak corresponding to a period of 94 s is more than three times the noise peaks, whereas the second

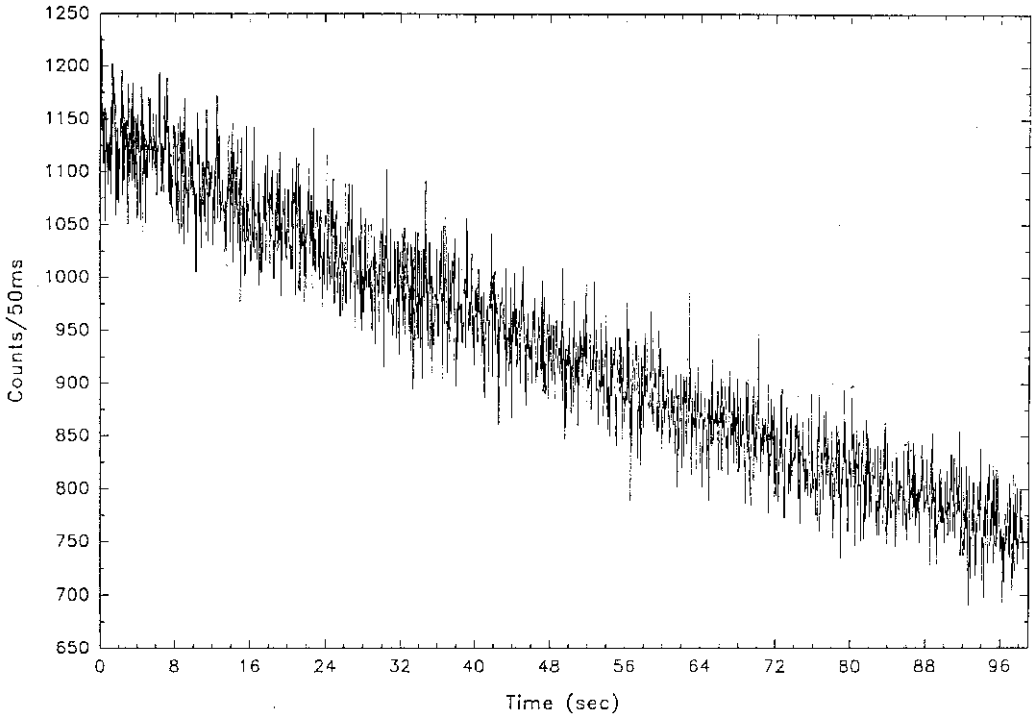

Figure 7. Plot of sky brightness data obtained during the evening twilight of 1995 October 23.

one appearing around the 43 s period is less than two times. A close inspection of Figure 7 indicates that the rate of reduction in sky brightness was greater in the initial stages than that at the later stages; the above two peaks could be arising out of this. Figure 8(b), which contains the DFT of the first half of the time series presented in Figure 7, does not show the above-mentioned peaks. The power spectrum of the subset is completely noisy with peaks of similar amplitudes appearing through out the entire frequency range considered. There is no concentration of power at any frequency, particularly at those frequencies which are prominent in the DFT of the coronal brightness data. These results rule out the possibility of the associated electronics modulating the input brightness at all or some of the periodicities identified in the coronal data.

The diaphragm which we used subtended an angle of 1.5 arc min in the sky and the brightness variation due to the effect of seeing, which could be in the range 2–3 arc sec, is expected to be small and random across the same. The intensity variations due to the seeing effects, usually, lie in the frequency range 5–10 Hz, and all the six components quoted above have much smaller frequencies (<0.2 Hz).

None of the periods given in Table I is associated with the gear system, which is fitted with an anti-backlash mechanism, used in the coelostat drive. The stepper motor rotated once in a second and the next gear coupled to it rotated once in 420 s.

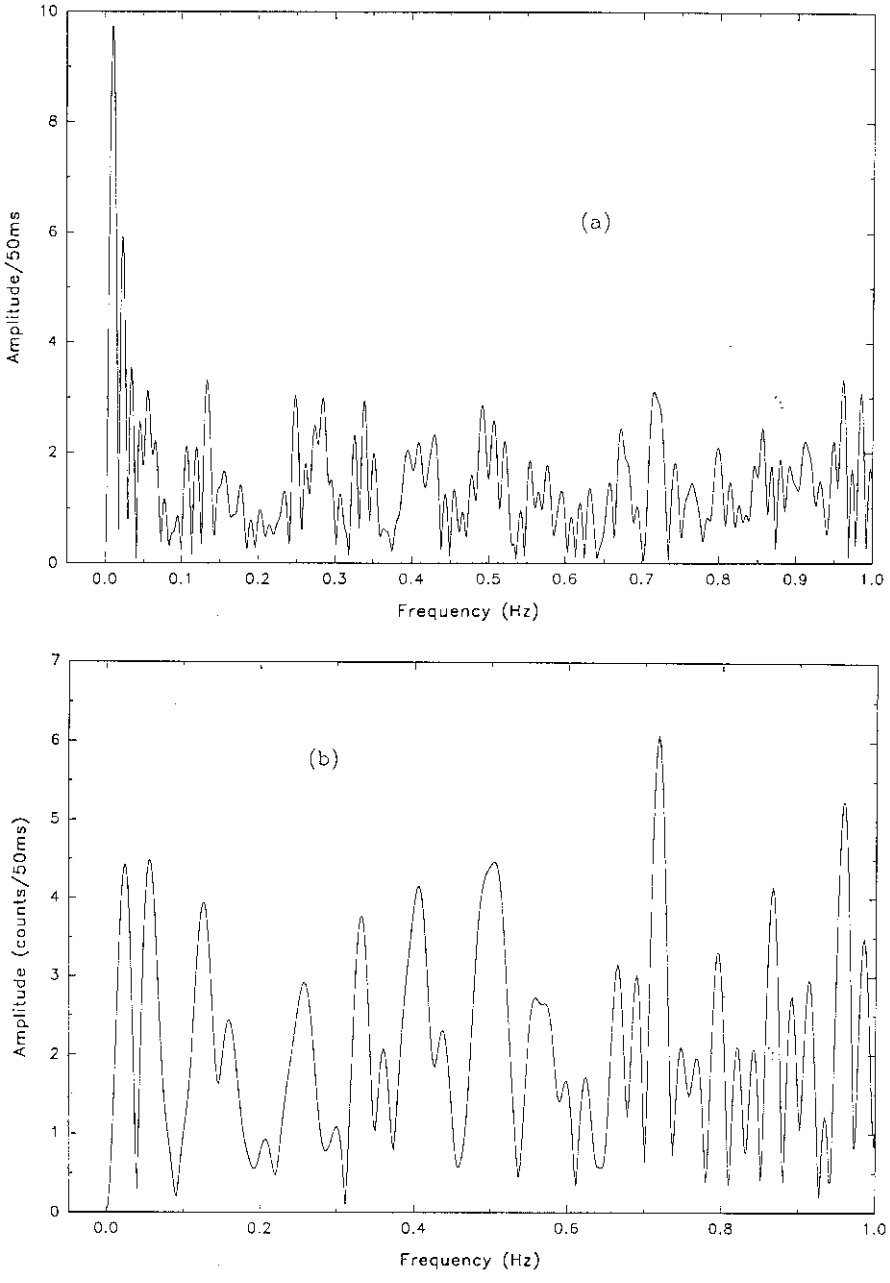

Figure 8a–b. (a) Amplitude spectrum of the entire time series shown in Figure 7. (b) Amplitude spectrum of the first 943 samples (approximately half) of the time series shown in Figure 7.

The coelostat mirror feeding the horizontal telescope rotated through an angle of 0.0375 arc sec every 5 ms with each step of the stepper motor, thereby producing an almost smooth tracking motion. Visually, it was found that the drift of the image with respect to the aperture was only because of the continuous change, which is negligible over one minute interval, in the declination of the Sun. A couple of weeks after the event we made a number of trials with the same experimental setup by positioning the aperture slightly away from the solar limb. This procedure provided an inhomogeneous sky background where the intensity decreased rapidly with increasing angular distance from the solar limb. Under such a condition any oscillations in the pointing of the telescope are expected to cause variations in the observed intensity. However, we could not detect any significant periodicity in the power spectra obtained from the data. Hence, it is unlikely that the spatial variations in the corona coupled with the telescope pointing variations caused the above frequency components. The motion of coronal features is likely to produce non-sinusoidal and also non-periodic variations in intensity.

The strong point in favour of attributing the above six component frequencies to the coronal oscillations is their extremely sinusoidal nature and near-coherence over the entire period of observation. We could determine their periods, amplitudes and input phases which facilitated the exact reconstruction of the data only because of these characteristics of the components. Further, no harmonics of significant amplitudes were seen in the power spectrum. It is difficult to understand why any variation associated with either atmospheric transparency, or seeing effects, or image motion, or blurring should cause such coherent oscillations of constant amplitudes over a minute interval. All the above sources are expected to cause variations, but of non-periodic and variable amplitudes. Here we stress that there is no reason to believe that the usual sources of error, most of which were taken care of, could produce such constant amplitude oscillations coherent over a minute interval; any variation caused by them should be either random or spiky in nature.

We conclude that the 6 dominant sinusoidal components identified and given in Table I are not produced by any extraneous agencies, but are the essential components of the coronal brightness variation.

The residuals obtained from the data after the removal of the contributions from the above 6 sinusoidal components are shown in Figure 9. The residuals, binned over 0.5 s, and the mean brightness level, derived from the least-square analysis, are also shown in the figure. The amplitude spectrum in the frequency range 0–10 Hz obtained from the residuals is plotted in Figure 10. The spectrum appears noisy. The two peaks appearing at 0.40 and 1.07 Hz have amplitudes around the threshold of 19.5 counts/50 ms mentioned above; the first one is significant at 99.98 and the second at 99.97% confidence levels. The several peaks with amplitudes around 16 counts/50 ms are significant at 99.68% confidence levels. We are not in a position to comment on the realities of these peaks; further observations are needed. To look for any short-lived oscillations we also did a piece-wise power spectrum analysis of the residuals after splitting the data into 5 segments of 188

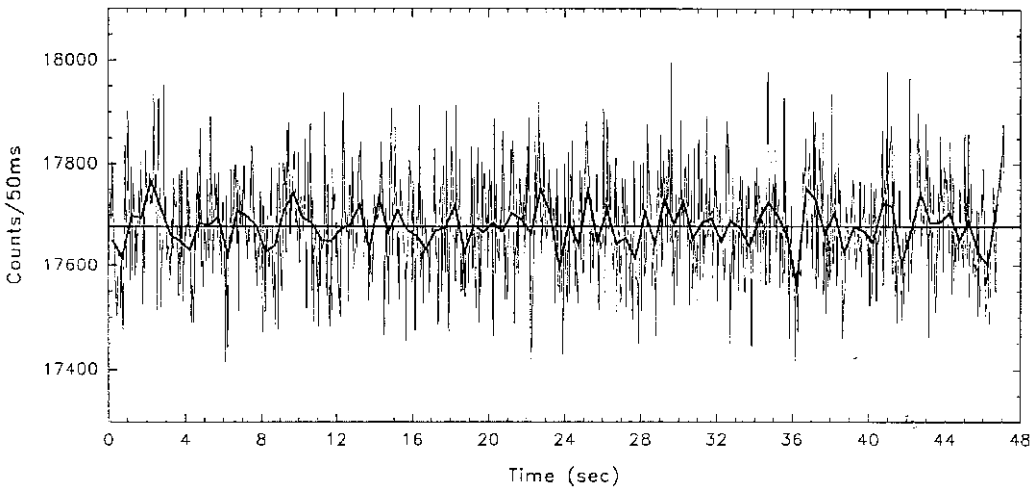

Figure 9. Thin, spiky line shows the plot of the residuals obtained from the data after the removal of all the 6 components given in Table I and the thick line the residuals after re-binning over 0.5 s. The mean brightness level obtained from the least-square analysis is also indicated. The time is reckoned as in Figure 1.

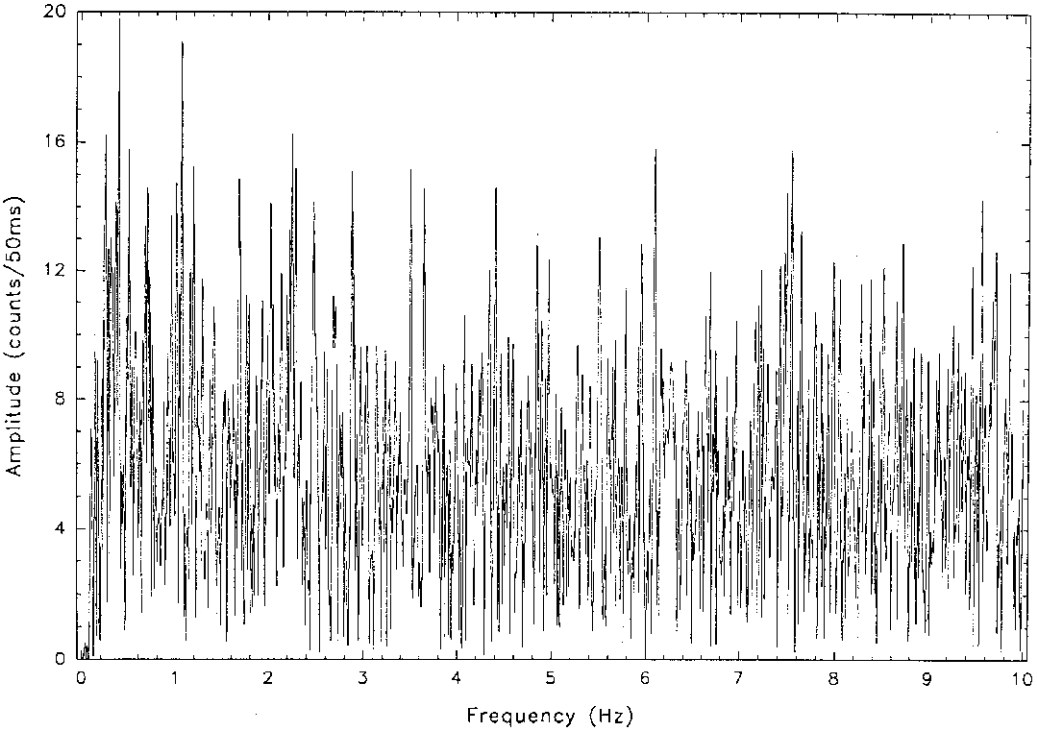

Figure 10. Amplitude spectrum in the frequency range 0–10 Hz computed from the residuals plotted in Figure 9.

Table II
Slow mode in quiet Sun, $C_s = 143$ km s^{-1}

P (s)	$\lambda = C_s P$ (cm)	δ_1^2/δ_0^2	F (ergs cm^{-2} s^{-1})
56.5	0.8×10^9	1.3×10^{-2}	9.6×10^3
19.5	2.8×10^8	2.7×10^{-3}	2.0×10^3
13.5	1.9×10^8	4.8×10^{-3}	3.5×10^3
8.0	1.1×10^8	2.6×10^{-3}	1.9×10^3
6.1	0.9×10^8	3.1×10^{-3}	2.2×10^3
5.3	0.8×10^8	2.0×10^{-3}	1.5×10^3

Table III
Slow mode in active regions, $C_s = 185$ km s^{-1}

P (s)	$\lambda = C_s P$ (cm)	δ_1^2/δ_0^2	F (ergs cm^{-2} s^{-1})
56.5	1.1×10^9	1.3×10^{-2}	5.2×10^5
19.5	3.6×10^8	2.7×10^{-3}	2.5×10^4
13.5	2.5×10^8	4.8×10^{-3}	4.5×10^4
8.0	1.5×10^8	2.6×10^{-3}	2.4×10^4
6.1	1.1×10^8	3.1×10^{-3}	1.2×10^4
5.3	1.0×10^8	2.0×10^{-3}	1.8×10^4

points each. The resulting power spectra were then added to reduce the effect of noise; however, we could detect no significant periodic components.

5. Modeling of Coronal Oscillations

Coronal structures are expected to undergo three types of oscillations – non-compressional Alfvén waves, and the compressional slow and fast magnetosonic waves. The restoring force in Alfvén oscillation is the magnetic tension whereas in the magnetosonic waves, the magnetic and kinetic pressures provide the restoring forces. It has been argued that all buoyancy effects related to gravitational forces can be neglected in the corona. The compressional modes may reveal themselves in the form of intensity oscillations through the variation of the emission measure. The Alfvénic oscillations are essentially the velocity oscillations and do not cause any density oscillations and since our data shows intensity oscillations, these could only be interpreted either as the slow mode or the fast mode. From theoretical studies of the coronal oscillations (Zirker, 1995; Porter, Klimchuk, and Sturrock, 1994, and references therein), one expects a wide range of periods of these oscillations.

It has been recently concluded by Porter, Klimchuk, and Sturrock (1994) that the fast magnetosonic waves have the right fluxes and dissipation rates to overcome the radiative losses. We have observed intensity oscillations with periods and

Table IV
Fast mode in quiet Sun, for $B \approx 2.4$ G and $V_A \approx 303$ km s^{-1}

P (s)	$\lambda \times 10^{-9}$	n	F (ergs cm^{-2} s^{-1})
56.5	1.7	4.0	1.0×10^5
19.5	0.6	11.6	2.0×10^4
13.5	0.4	16.8	3.3×10^4
8.0	0.3	28.0	1.8×10^4
6.1	0.2	37.6	2.2×10^4
5.3	0.2	43.0	1.4×10^4

Table V
Fast mode in active regions, for $B \approx 34$ G and $V_A \approx 1754$ km s^{-1}

P (s)	$\lambda \times 10^{-9}$	n	F (ergs cm^{-2} s^{-1})
56.5	10.3	0.7	
19.5	3.4	2.0	2.2×10^7
13.5	2.4	3.0	3.8×10^7
8.0	1.4	5.0	2.0×10^7
6.1	1.0	6.6	2.5×10^7
5.3	0.9	7.4	1.6×10^7

amplitudes as given in Table I. In order to identify these waves, we choose canonical parameters for the quiet and active region of the Sun from Porter, Klimchuk, and Sturrock (1994). The most unknown parameter in the model is the wavelength of the oscillations. For a system to support oscillations, the size of the system must be equal or larger than the wavelength of the oscillations. In the absence of spatial resolution required to discern these oscillations, one can surmise that there are regions with sizes of the order of a wavelength and all these regions are oscillating with some degree of coherence among them giving a net oscillatory contribution to the intensity. Thus, we parametrize the wavelength λ of the oscillations as $\lambda = L/n$, where L is the size of the observed region and n can be interpreted as the number of separate smaller regions in it. For the quiet Sun, we take the electron density $n_e = 5 \times 10^8$ cm^{-3} at 1.25 solar radii, the magnetic field $B = 3$ G, the electron temperature $T_e = 1.5 \times 10^6$ K. This gives the sound speed $C_s = 143$ km s^{-1} and the Alfvén speed $V_A = 378$ km s^{-1}. Assuming that the observed oscillations are slow modes with dispersion relation $\lambda = C_s P$, where P is the period of the wave, we estimate the wavelength and the fluxes for all the observed periods and these are given in Table II. Similarly choosing the parameters of active region as $n_e = 3.0 \times 10^9$ cm^{-3}, $T_e = 2.5 \times 10^6$ K, $B = 100$ G, we list the results for wavelengths and fluxes for the active region in Table III. The flux is given by

$F = \frac{1}{2}\delta_0(V_1^2/C_s^2)C_s^3$, where δ_0 is the mean density, and $V_1^2/C_s^2 = \delta_1^2/\delta_0^2 =$ amplitude of intensity modulation and is estimated by dividing the amplitude given in Table I by the mean count ∼17677. In this case the sound speed $C_s = 185\,\mathrm{km\,s^{-1}}$ and the Alfvén speed $V_\mathrm{A} = 5150\,\mathrm{km\,s^{-1}}$.

The identification of the observed oscillation with the fast magnetosonic waves is a little more tricky. Here we attempt to estimate the magnetic field from the observed periods. The dispersion relation for the fast modes is given as $\lambda = PV_\mathrm{A} = L/n$. Assuming the magnetic field B to be the same for all the periods, we estimate the fluxes and the value of n and present them in Table IV for the quiet Sun and Table V for active region. The flux F in this case is given by $F = \frac{1}{2}\delta_0 V_\mathrm{A}^3(V_1^2/V_\mathrm{A}^2)$ and $V_1^2/V_\mathrm{A}^2 = (\delta_1/\delta_0)^2 =$ fractional amplitude of intensity modulation and is estimated by dividing the amplitude given in Table I by the mean count ≈ 17677.

The flux for the wave with period $P = 56.5$ s is not determined since the region under observations, i.e., a region of 1.5 arc min width cannot support even one complete oscillation. From the above estimates, it follows that fast mode in active region can provide enough flux for the heating of the corona as also concluded by Porter, Klimchuk, and Sturrock (1994).

6. Conclusion

We have observed coronal intensity oscillations of periods ranging from 5.3 to 56.5 s. If these oscillations are identified with the fast magnetosonic mode, they provide enough flux for the heating of the active regions in the solar corona. We plan to continue the study of oscillations with enough resolution to delineate the size of the oscillating region and to observe at different solar radii to detect changes in oscillations with radius, if any.

Acknowledgements

We thank the local administration at Kalpi for permitting us to set up camp at Gram Udyog building and for their co-operation. We also thank all our colleagues of Indian Institute of Astrophysics for their help in planning the expedition.

References

Cargill, P. J.: 1995, in J. R. Kuhn and M. J. Penn (eds.), *Infrared Tools for Solar Astrophysics: What is Next?*, World Scientific Publishing Co. Ltd., Singapore, p. 17.
Deeming, T. J.: 1975, *Astrophys. Space Sci.* **36**, 137.
Groth, E. J.: 1975, *Astrophys. J. Suppl.* **29**, 285.
Hollweg, J.: 1981, *Solar Phys.* **70**, 25.
Ionson, J. A.: 1978, *Astrophys. J.* **226**, 650.
Koutchmy, S., Zugzda, Y. D., and Locans, V.: 1983, *Astron. Astrophys.* **120**, 185.

Liebenberg, D. H. and Hoffman, M. M.: 1974, in G. Newkirk (ed.), 'Coronal Disturbances', *IAU Symp.* **57**, 485.
Pasachoff, J. M. and Ladd, E. F.: 1987, *Solar Phys.* **109**, 365.
Pasachoff, J. M. and Landman, D. A.: 1984, *Solar Phys.* **90**, 325.
Porter, L. J., Klimchuk, J. A., and Sturrock, P. A.: 1994, *Astrophys. J.* **435**, 482.
Rušin, V. and Minarovjech, M.: 1991, in P. Ulmschneider, E. R. Priest, and R. Rosner (eds.), *Mechanisms of Chromospheric and Coronal Heating*, Springer-Verlag, Berlin, p. 30.
Stein, R. F. and Leibacher, J.: 1974, *Ann. Rev. Astron. Astrophys.* **12**, 407.
Zirker, J. B.: 1995, in J. R. Kuhn and M. J. Penn (eds.), *Infrared Tools for Solar Astrophysics: What is Next?*, World Scientific Publishing Co. Ltd., Singapore, p. 13.